NASA/TM-2001-210863

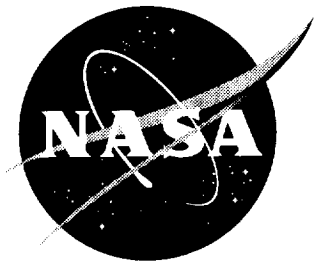

# Equivalent-Continuum Modeling of Nano-Structured Materials

*Gregory M. Odegard and Thomas S. Gates*
*Langley Research Center, Hampton, Virginia*

*Lee M. Nicholson*
*ICASE*
*Langley Research Center, Hampton, Virginia*

*Kristopher E. Wise*
*Langley Research Center, Hampton, Virginia*

National Aeronautics and
Space Administration

Langley Research Center
Hampton, Virginia 23681-2199

May 2001

Available from:

NASA Center for AeroSpace Information (CASI)
7121 Standard Drive
Hanover, MD 21076-1320
(301) 621-0390

National Technical Information Service (NTIS)
5285 Port Royal Road
Springfield, VA 22161-2171
(703) 605-6000

# Equivalent-Continuum Modeling of Nano-Structured Materials

*Gregory M. Odegard*[*], *Thomas S. Gates, Lee M. Nicholson*[§], *and Kristopher E. Wise*[*]

*NASA Langley Research Center, Hampton, Virginia*

## Abstract

A method has been developed for modeling structure-property relationships of nano-structured materials. This method serves as a link between computational chemistry and solid mechanics by substituting discrete molecular structures with an equivalent-continuum model. It has been shown that this substitution may be accomplished by equating the vibrational potential energy of a nano-structured material with the strain energy of representative truss and continuum models. As an important example with direct application to the development and characterization of single-walled carbon nanotubes, the model has been applied to determine the effective continuum geometry of a graphene sheet. A representative volume element of the equivalent-continuum model has been developed with an effective thickness. This effective thickness has been shown to be similar to, but slightly smaller than, the interatomic spacing of graphite.

KEY WORDS: nanotechnology, nanotubes, continuum mechanics, molecular mechanics, finite elements

## Nomenclature

Graphite orientation

$a_\beta$ - Unit-cell base axes
$D$ - Graphite orientation indicator
$n_\beta$ - Orientation integers

Force field

$E^{el}$ - Non-bonded electrostatic potential energy
$E^{g}$ - Vibrational potential energy of graphene sheet
$E^{m}$ - Potential energy of nano-structured material
$E^{vdW}$ - Non-bonded van der Waals potential energy
$E^{\theta}$ - Bond-angle variation potential energy
$E^{r}$ - Bond stretching potential energy
$E^{\tau}$ - Bond torsion potential energy
$E^{\omega}$ - Bond inversion potential energy
$K_i^r$ - Constant associated with C-C bond stretching in graphite
$K_i^\theta$ - Constant associated with C-C-C bond-angle variation in graphite
$\theta_i$ - Deformed bond-angle of C-C-C bonds in graphite

---

[*] National Research Council, NASA Langley Research Center
[§] ICASE, Structures and Materials Division, NASA Langley Research Center

$\Theta_i$ - Equilibrium bond-angle of C-C-C bonds in graphite

$\rho_i$ - Deformed bond length of C-C bonds in graphite

$P_i$ - Equilibrium bond length of C-C bonds in graphite

Truss and continuum models

$a$ - Elastic rod type of outer portion of truss representative volume element

$A_i^j$ - Cross-sectional area of rod $i$ of truss member type $j$

$A^{nt}$ - Cross sectional area of carbon nanotube

$b$ - Elastic rod type of inner portion of truss representative volume element

$r_i^j$ - Deformed distance between joints of rod $i$ of truss member type $j$

$R_i^j$ - Undeformed distance between joints of rod $i$ of truss member type $j$

$t$ - Wall thickness of continuum nanotube

$Y^g$ - Young's modulus of graphene sheet

$Y_i^j$ - Young's modulus of rod $i$ of truss member type $j$

$Y^{nt}$ - Young's modulus of carbon nanotube

$r'$ - Mid-plane radius of continuum nanotube wall

$r''$ - Inner radius of continuum nanotube wall

$r'''$ - Outer radius of continuum nanotoube wall

$\Lambda^c$ - Mechanical strain energy of the continuum model

$\Lambda^t$ - Mechanical strain energy of the truss model

$\nu^g$ - Poison's ratio of graphene sheet

Boundary conditions

$B_1..B_{10}$ - Displacement field constants

$d_k^{(\alpha)}$ - Vector of periocity of representative volume element face $\alpha$

$f_k$ - RVE and macroscopic coordinate system offset vector

$h$ - Height of macroscopic graphene plate

$u_k^{(\alpha)}$ - Displacement vector of representative volume element face $\alpha$

$\hat{u}_k$ - Global displacement vector

$w$ - Width of macroscopic graphene plate

$x_k$ - Cartesian coordinate system of the representative volume element

$\hat{x}_k$ - Global coordinate system

$\alpha$ - Representative volume element face number

$\Delta$ - Prescribed displacement applied to macroscopic plate

$\varepsilon_{kl}$ - Strain tensor

$\sigma_{kl}$ - Stress tensor

# 1. Introduction

Nano-structured materials have excited considerable interest in the materials research community in the last few years partly due to their potentially remarkable mechanical properties [1]. In particular, materials such as carbon nanotubes, nanotube and nanoparticle-reinforced polymers and metals, and nano-layered materials have shown considerable promise. For example, carbon nanotubes could potentially have a Young's modulus as high as 1 TPa and a tensile strength approaching 100 GPa. The design and fabrication of these materials are performed on the nanometer scale with the ultimate goal to obtain highly desirable macroscopic properties.

One of the fundamental issues that needs to be addressed in modeling macroscopic mechanical behavior of nano-structured materials based on molecular structure is the large difference in time and length scales. On the opposite ends of the time and length scale spectrum are computational chemistry and solid mechanics, each of which consists of highly developed and reliable modeling methods. Computational chemistry models predict molecular properties based on known quantum interactions, and computational solid mechanics models predict the macroscopic mechanical behavior of materials idealized as continuous media based on known bulk material properties. However, a corresponding model does not exist in the intermediate time and length scale range. If a hierarchical approach is used to model the macroscopic behavior of nano-structured materials, then a methodology must be developed to link the molecular structure and macroscopic properties. Even though there is a long history of modeling bulk properties of materials based on molecular properties, a simple link between the firmly established disciplines of computational chemistry and solid mechanics has not been established.

In this paper, a methodology for linking computational chemistry and solid mechanics models has been developed. This tool allows molecular properties of nano-structured materials obtained through molecular mechanics models to be directly used in determining the corresponding bulk properties of the material at the macroscopic scale. The advantages of the proposed method are its simplicity and direct connection with computational chemistry and solid mechanics.

This approach consists of two major steps. First, the chemical structure and vibrational potential energy function of the nano-structured material, which is determined from computational chemistry, is used to obtain an equivalent mechanical pin-jointed truss model. Second, the truss representation of the nano-structured material is substituted with an equivalent-continuum model. The mechanical behavior of the continuum model closely approximates that of the nano-structured material.

As an important example, with direct application to the development and characterization of single-walled carbon nanotubes (SWNT), the proposed method has been used to determine the effective geometry of a graphene sheet. A representative volume element (RVE) of the graphene layer has been modeled as a continuous plate with an effective thickness that has been determined from the nano-structured properties of graphite by using the proposed method.

## 2. Background and basic concepts

A discussion of some of the necessary background and concepts associated with characterization and modeling of carbon nanotubes is required for the development of the proposed method.

### 2.1 Carbon nanotubes

Carbon nanotubes have become a primary focus in nanotechnology research due to their exceptionally high stiffness and strength. One of the fundamental issues scientists are confronting is the characterization of the mechanical behavior and properties of individual carbon nanotubes. Many experimental [2-6] and theoretical [7-11] studies have been performed on single- and multi-walled carbon nanotubes. In particular, deformation modes and overall tube stiffnesses have been closely examined.

In order experimentally characterize the mechanical behavior of nanotubes, a thorough understanding of the physical properties, such as effective cross-sectional area and moment of inertia, and materials properties, such as Young's modulus and Poisson's ratio, is necessary. These quantities are traditionally associated with the macroscopic scale, where the characteristic dimensions of a continuum solid are well defined. The determination of these properties has been attempted in many of the studies cited above without proper regard to an acceptable definition of the nanotube geometry. Accurate values of macroscopic physical and mechanical properties are crucial in establishing a meaningful link between nanotube properties and the properties of larger structures, such as nanotube-reinforced polymer composites. Therefore, caution should be used when applying continuum-type properties to nano-structured materials.

In many studies, it has been assumed that the nanotube "wall thickness" is merely the interatomic spacing of two or more graphene sheets [3, 6-11], which is about 0.34 nm in single-crystal graphite. While this simple idealization appears to have intuitive merit, it does not necessarily reflect the *effective* thickness that is representative of continuum properties. In order to avoid this problem, Hernandez *et al.* [8] proposed the use of a specific Young's modulus, i.e., Young's modulus per unit thickness. Even though this approach is convenient for studies concerned with the relative stiffnesses of nanotubes, it is of little use when modeling a nanotube as a continuum structure. Another proposed solution to this dilemma is to assume that the nanotube is a solid cylinder [12-14]. This method is certainly convenient, however, significant inconsistencies arise when comparing moduli data of single wall nanotubes (SWNT) and multi-walled nanotubes (MWNT) when both are assumed to be a solid cylinder.

A continuum modeling approach, which relies on an effective wall thickness, was proposed by Yakobson *et al.* [15]. They developed an elastic continuous shell model to represent a carbon nanotube. In their model, a wall thickness (0.066 nm) was calculated based on an assumed value of Young's modulus of the nanotube (5.5 TPa). This approach is extremely useful in deformation analysis of nanotubes (e.g., buckling), however, it is not convenient when attempting to calculate the modulus of the nanotube based on empirical or theoretical data where the thickness is not known *a priori*. Govindjee and Sackman [14] utilized the Bernoulli-Euler beam theory to show that for a MWNT in bending, a large number of atomic layers are necessary in order to be able to assume that the cross-section of the nanotube is a continuum. This type of

approach assumes that the nanotube is a solid cylinder instead of using a more realistic model of single or multiple hollow cylinders with inter-wall interactions. Ru [16] used an elastic shell continuum model to investigate buckling of double-walled nanotubes subjected to axial compression. It was shown that the van der Waals forces between the layers did not increase the critical axial strains that correspond to buckling. Specific thicknesses for the inner and outer walls were not discussed in detail. Ru [17] proposed that the effective bending stiffness of SWNT should be regarded as an independent material parameter not related to the bending stiffness associated with the Bernoulli-Euler beam bending theory. This simplification was suggested in order to explain inconsistencies associated with the use of the classical bending formula for SWNT using a wall thickness of 0.34 nm.

It has been postulated by Cornwell and Wille [12] and Robertson *et al.* [18] that the strain energy induced by bending a flat graphene sheet into a circular nanotube causes an increase in the apparent stiffness of the tube as a function of the nanotube radius. Conversely, Halicioglu [19] has shown that significant radial and circumferential stresses are present in the nanotube that are also dependent on the tube radius. Therefore, it follows that in order to properly model the mechanical behavior of a SWNT using continuum mechanics, the effective geometry must be known. If the nanotube is modeled as a continuous hollow cylinder with an effective wall thickness, then a simple first step is to model the flat graphene sheet in order to determine the effective wall thickness. In the current study, the effective thickness will be calculated as an example of the proposed approach.

### 2.2 Notation for graphite orientation

In order to clarify some of the notation used in this paper, a brief description of the commonly used notation for graphite is necessary. A graphene sheet is composed of bonded carbon atoms arranged in a repeating array of regular hexagons (Figure 1). The simplest way of specifying the orientation of a graphite structure is in terms of a vector $D$ that joins two equivalent points (atoms) of the graphene sheet. The vector may be expressed as:

$$D = n_\beta \mathbf{a}_\beta \tag{1}$$

where the index $\beta = 1,2$; $\mathbf{a}_\beta$ are the unit-cell base vectors of the graphene sheet (Figure 1); $n_\beta$ is a set of integers where $n_1 \geq n_2$; and the summation convention is used for repeated indices. It is common to express equation (1) in terms of the integers as the ordered pair $(n_1,n_2)$.

### 2.3 Representative volume element

To reduce the time and number of computations associated with modeling the graphene sheet, a representative volume element (RVE) for graphene was used in this study (Figure 2). The selected RVE allows each degree of freedom of the carbon atom associated with bond stretching and bond-angle variation in the hexagonal ring to be completely modeled by truss and continuum finite element model nodal-displacement degrees of freedom. Also, this RVE allows the displacements on the boundary of the proposed chemical, truss, and continuum models to correspond exactly. Furthermore, macroscopic loading conditions applied to a continuous

graphene plate can be easily reduced to periodic boundary conditions that are applied to the RVE.

## 3. Modeling procedure

The proposed method of modeling nano-structured materials with an equivalent-continuum is outlined below. The approach uses the energy terms that are used in molecular mechanics modeling for the development of a continuum solid. Therefore, a brief description of molecular mechanics is given first followed by an outline of the equivalent-truss and equivalent-continuum model development.

### 3.1 Molecular mechanics

An important component in molecular mechanics calculations of the nano-structure of a material is the description of the forces between individual atoms. This description is characterized by a force field. In the most general form, the total potential energy of the force field for a nano-structured material is described by the sum of many individual energy contributions:

$$E^m = E^{\rho} + E^{\theta} + E^{\tau} + E^{\omega} + E^{vdW} + E^{el} \tag{2}$$

where $E^{\rho}$, $E^{\theta}$, $E^{\tau}$, and $E^{\omega}$ are the energies associated with bond stretching, angle variation, torsion, and inversion, respectively. The non-bonded interaction energies consist of van der Waals, $E^{vdW}$, and electrostatic, $E^{el}$, terms. Various functional forms may be used for these energy terms depending on the particular material and loading conditions considered [20]. Obtaining accurate parameters for a force field amounts to fitting a set of experimental or calculated data to the assumed functional form, specifically, the force constants and equilibrium structure. In situations where experimental data are either unavailable or very difficult to measure, quantum mechanical calculations can be a critical source of information for defining the force field.

### 3.2 Truss model

Due to the nature of the molecular force field, a pin-jointed truss model may be used to represent the energies given by equation (2) where each truss member represents the forces between two atoms. Therefore, a truss model allows the mechanical behavior of the nano-structured system to be accurately modeled in terms of displacements of the atoms. This mechanical representation of the lattice behavior then serves as an intermediate step between linking the vibrational potential with an equivalent-continuum model. In the truss model, each truss element corresponds to a chemical bond or a significant non-bonded interaction. The stretching potential of each bond corresponds with the stretching of the corresponding truss element. Traditionally, atoms in a lattice have been viewed as masses that are held in place with atomic forces that resemble elastic springs [21]. Therefore, bending of truss elements is not needed to simulate the chemical bonds, and it is assumed that each truss joint is pinned, not fixed.

The mechanical strain energy, $\Lambda^t$, of the truss model is expressed in the form:

$$\Lambda^t = \sum_j \sum_i \frac{A_i^j Y_i^j}{2R_i^j}\left(r_i^j - R_i^j\right)^2 \tag{3}$$

where $A_i^j$ and $Y_i^j$ are the cross-sectional area and Young's modulus of rod $i$ of truss member type $j$, respectively. The term $r_i^j - R_i^j$ is the stretching of rod $i$ of truss member type $j$, where $R_i^j$ and $r_i^j$ are the undeformed and deformed lengths of the truss elements, respectively. For equation (3), as well as all equations up through section 4.2, the summation convention for repeated indices is not used.

In order to represent the chemical behavior with the truss model, equation (3) must be equated with equation (2) in a physically meaningful manner. Each of the two equations are sums of energies for particular degrees of freedom. The main difficulty in the substitution is specifying equation (3), which has stretching terms only, for equation (2), which also has bond-angle variance and torsion terms. No generalization can be made for overcoming this difficulty for every nano-structured system. A feasible solution must be determined for a specific nano-structured material depending on the geometry, loading conditions, and degree of accuracy sought in the model.

### 3.3 Equivalent-continuum model

For many years, researchers have developed methods of modeling large-area truss structures with equivalent-continuum models [22-27]. These studies indicate that various methods and assumptions have been employed in which equivalent-continuum models have been developed that adequately represent truss structures. In this study, the truss and continuum models are assumed to be equivalent under the following conditions:

1. Truss lattices with pinned joints can be modeled accurately with an equivalent-continuum model that is based on classical continuum mechanics. For this case, micropolar [28] continuum assumptions are not necessary.
2. The models have the same degrees of freedom.
3. The displacements along the edges of the RVE are identical for the two models subjected to the same static loading conditions.
4. The same amount of thermoelastic strain energy is stored in the two models when deformed by identical static loading conditions.

If these criteria are satisfied, then a particular continuum model, such as a beam, plate, shell, or three-dimensional solid, may be directly substituted for a discrete truss lattice. The parameters of the solid, such as the elastic properties and geometry, are determined based on the above criteria. In some cases the strain energy of the continuum, $\Lambda^c$, can be easily formulated analytically and compared directly with equation (3) to obtain the equivalent-continuum

properties. In other cases, especially with complex geometries and deformations, numerical tools need to be used to determine the continuum parameters.

Once an equivalent-continuum model has been determined, the mechanical behavior of larger structures made of the nano-structured material may be predicted using the standard methods of continuum mechanics.

## 4. Example: effective geometry of a graphene sheet

In this section, a graphene sheet is modeled as a continuous plate with a finite thickness that represents the effective thickness for the determination of continuum-type mechanical and physical properties. By using the methodology described above, the molecular mechanics model is substituted with a truss model and subsequently an equivalent-plate model. The continuum model may then be used in further solid mechanics-based analyses of SWNT.

### 4.1 Molecular mechanics model

The force constants used in this example were taken from the MM3 force field of Allinger and coworkers [29-31]. Due to the nature of the material and loading conditions in the present study, only the bond stretching and bond-angle variation parameters were used. Torsion, inversion, and non-bonded interactions were assumed to be negligible for the case of a graphene lattice subjected to small deformations. For this example, the vibrational potential energy of a graphene sheet with carbon-to-carbon bonds is expressed as a sum of simple harmonic functions:

$$E^s = \sum_i K_i^\rho \left(\rho_i - \mathrm{P}_i\right)^2 + \sum_i K_i^\theta \left(\theta_i - \Theta_i\right)^2 \tag{4}$$

where the terms $\mathrm{P}_i$ and $\Theta_i$ refer to the undeformed interatomic distance of bond $i$ and the undeformed bond-angle $i$, respectively. The quantities $\rho_i$ and $\theta_i$ are the distance and bond-angle after stretching and angle variance, respectively (see Figure 3). $K_i^\rho$ and $K_i^\theta$ are the force constants associated with the stretching and angle variance, respectively, of the chemical bonds. Using the parameters for the MM3 force field [29-31], the force constants used in this example are:

$$\begin{aligned} K_i^\rho &= 46900 \frac{kcal}{mole \cdot nm^2} = 3.26 \cdot 10^{-7} \frac{nJ}{bond \cdot nm^2} \\ K_i^\theta &= 63 \frac{kcal}{mole \cdot rad^2} = 4.38 \cdot 10^{-10} \frac{nJ}{angle \cdot rad^2} \end{aligned} \tag{5}$$

and the equilibrium bond length, $\mathrm{P}_i$, is 0.140 nm.

### 4.2 Truss model

Since it is difficult to express the mechanical strain energy, $\Lambda^t$, of the truss model in terms of the variable truss joint angles that are specified in molecular mechanics ($\theta_i$-$\Theta_i$), the RVE has been instead modeled with extra rods between nearly adjacent joints to represent the interaction between the corresponding carbon atoms (Figure 3). In order to represent the chemical model, which has bond stretching and variable angles as degrees of freedom, with a truss model that has stretching degrees of freedom only, two types of elastic rods, *a* and *b*, are incorporated into the truss RVE.

The mechanical strain energy, $\Lambda^t$, of the discrete truss system in Figure 3 is expressed in the form of equation (3):

$$\Lambda^t = \sum_i \frac{A_i^a Y_i^a}{2R_i^a}\left(r_i^a - R_i^a\right)^2 + \sum_i \frac{A_i^b Y_i^b}{2R_i^b}\left(r_i^b - R_i^b\right)^2 \tag{6}$$

where the superscripts correspond to rod types *a* and *b*, respectively. Comparing equations (4) and (6), it is clear that the bond stretching term in the equation (4) can be related to the first term of equation (6) for the rods of type *a*:

$$K^\rho = \frac{A_i^a Y_i^a}{2R_i^a} \tag{7}$$

where it is assumed that $\rho_i = r_i^a$ and $P_i = R_i^a$. However, the second terms in equations (4) and (6) cannot be related directly. In order to equate the constants, the chemical bond-angle variation must be expressed in terms of the elastic stretching of the truss elements of type *b*. For simplicity, it may be assumed that the prescribed loading conditions consist of small, elastic deformations only. This assumption is not an over-simplification for the graphene sheet since the deformations for highly stiff linear-elastic materials subjected to many practical loading conditions are quite small.

In order to express the Young's modulus of the rods of type *b* in terms of the bond-angle constant, a simple analysis of the deformation was performed (Figure 4). For small deformations of the hexagonal RVE, changes in the bond-angles are small. Therefore, in the second terms of equations (4) and (6), it can be assumed that $r_i^a = R_i^a$ and that small angle approximations are valid. With these assumptions it can be shown that:

$$\theta_i - \Theta_i \approx \frac{r_i^b - R_i^b}{2R_i^a} \tag{8}$$

Substitution of equation (8) into equations (4) and (6) results in the following approximation:

$$K_i^{\theta} = \frac{2}{3} R_i^h A_i^h Y_i^h \tag{9}$$

Therefore, the Young's moduli of the two rod types are:

$$Y_i^a = \frac{2K_i^{\rho} R_i^a}{A_i^a} \quad Y_i^h = \frac{3K_i^{\theta}}{2R_i^h A_i^h} \tag{10}$$

The strain energy of the truss model may be expressed as:

$$\Lambda^t = \sum_i K^{\rho} \left(r_i^a - R_i^a\right)^2 + \sum_i \frac{3K^{\theta}}{4(R_i^h)^2} \left(r_i^h - R_i^h\right)^2 \tag{11}$$

Thus, the strain energy of the truss model is expressed terms of the vibrational potential energy constants.

### 4.3 Equivalent-plate model

Working with the assumptions discussed herein, the next step in linking the molecular and continuum models is to replace the equivalent-truss model with an equivalent-continuous plate with a finite thickness (Figure 3). This replacement is accomplished by determining and equating the strain energies of the truss and continuum models for a specific set of applied loads. For the case of the RVE shown in Figure 2, a direct solution of strain energy of the equivalent plate in terms of displacements is quite difficult to obtain in closed form. A simple and accurate way of calculating the strain energy of the truss and continuum RVE representations is to model them numerically by using the finite element method [32]. For a given set of loading conditions, the strain energies of the two models may then be quickly calculated and compared. Once this is accomplished, then the finite thickness of the equivalent plate is determined, and therefore, the effective thickness of a graphene sheet is known.

In order to satisfy the first condition of the criteria specified in section 3.3, it was assumed that the equivalent plate may be modeled using plate-like finite elements. To satisfy the second condition, it was assumed that the nodes of the two models are located at the same points, with the same degrees of freedom. A simple configuration that satisfies this requirement is shown in Figure 3, where the finite element nodes are located at each truss joint on the RVE edges (the intersections of the type *h* rods are not joined) and at the corners of the 4-noded equivalent-plate elements. These nodes are allowed to translate in the $x_1$ and $x_2$ directions only (The origin of the coordinates is indicated in Figure 3 and located at the centroid of the RVE). Therefore, the degrees of freedom of the two models are identical. For condition 3, the displacement gradients of the truss elements and the edges of the continuum elements were assumed to be linear. Finally, to satisfy condition 4, the two finite element models were subjected to identical loading conditions with the total strain energies calculated based on the nodal displacements. This step was performed iteratively while optimizing the plate thickness, which was the only available adjustable parameter. The corresponding plate thickness is the assumed effective thickness of the graphene sheet.

While the mechanical properties of the truss elements have been determined as described above, those of the graphene sheet were taken from the literature. Reliable values of the in-plane mechanical properties of graphite have been known for quite some time since they can be measured macroscopically, i.e., without any assumptions regarding the graphene sheet thickness. For this example, typical values of the mechanical properties were used [33-35]:

$$\begin{aligned} Y^g &= 1030\,\text{GPa} \\ \nu^g &= 0.170 \end{aligned} \tag{12}$$

where $Y^g$ and $\nu^g$ are Young's modulus and Poisson's ratio of graphite, respectively.

### 4.4 Boundary conditions

In order to determine an effective plate thickness, the truss and continuum models were subjected to three sets of identical loading conditions for each strain energy calculation. For each set of loading conditions, a corresponding effective thickness was determined. The loading conditions correspond to the three fundamental in-plane deformations of a plate, that is, uniform axial tension along $x_1$ and $x_2$ and pure shear loading. It was assumed that these loading conditions were applied to a macroscopic graphene sheet, i.e. a graphite sheet that has dimensions on the macroscopic scale so that there are a very large number of RVEs contained within the entire sheet. In order to numerically calculate the strain energy of the RVE under these loading conditions, the corresponding periodic boundary conditions for the these fundamental loadings were determined and applied to the macroscopic graphene sheet.

Using the method developed by Whitcomb *et al.* [36] and Chapman and Whitcomb [37] for woven composites, the boundary conditions for the graphene RVE (Figure 2) was determined in terms of the overall macroscopic displacement field. The periodic displacement conditions for the graphene RVE are given by:

$$u_k^{(\alpha)}\left(x_m + d_m^{(\alpha)}\right) = u_k^{(\alpha)}\left(x_m\right) + d_l^{(\alpha)} \frac{\partial \hat{u}_k}{\partial x_l} \tag{13}$$

where $u_k^{(\alpha)}$ is the displacement of a specific RVE face; $d_k^{(\alpha)}$ is the vector of periodicity; $\hat{u}_k$ is the macroscopic, volume-averaged displacement; $x_l$ is the RVE coordinate system located at the centroid of the RVE (Figure 3); the superscript $\alpha$ is the RVE face under consideration; and the subscripts $k,l,m = 1,2$, where repeated indices imply summation over the range of the index. The vector of periodicity is any vector that connects two equivalent points in a periodic array. The vectors of periodicity of particular interest here are those that connect points in adjacent RVEs. Figure 5 shows the vectors of periodicity for each set of faces of the RVE. It should be noted that $d_k^{(1)}$ is parallel to $a_2$ and $d_k^{(3)}$ is parallel to $a_1$ (see Figures 1 and 5). The vectors of periodicity for each face are defined with respect to the $x_k$ coordinate system by:

$$d_k^{(1)} = \left( \frac{R_i^a \sqrt{3}}{2}, \frac{3R_i^a}{2} \right)$$
$$d_k^{(2)} = \left( -\frac{R_i^a \sqrt{3}}{2}, \frac{3R_i^a}{2} \right) \tag{14}$$
$$d_k^{(3)} = \left( R_i^a \sqrt{3}, 0 \right)$$

Substitution of equation (14) and the geometry of the RVE into equation (13) gives the following constraints that represent the periodic boundary conditions for each group of opposing faces in the graphene RVE:

$$u_k^{(1)}\left( -\sqrt{3}x_2 - \frac{R_i^a \sqrt{3}}{2}, x_2 + \frac{3R_i^a}{2} \right) = u_k^{(1)}\left( -\sqrt{3}x_2 - \sqrt{3}R_i^a, x_2 \right) + \frac{R_i^a \sqrt{3}}{2}\left( \frac{\partial \hat{u}_k}{\partial x_1} \right) + \frac{3R_i^a}{2}\left( \frac{\partial \hat{u}_k}{\partial x_2} \right)$$
$$u_k^{(2)}\left( \sqrt{3}x_2 + \frac{R_i^a \sqrt{3}}{2}, x_2 + \frac{3R_i^a}{2} \right) = u_k^{(2)}\left( \sqrt{3}x_2 + \sqrt{3}R_i^a, x_2 \right) - \frac{R_i^a \sqrt{3}}{2}\left( \frac{\partial \hat{u}_k}{\partial x_1} \right) + \frac{3R_i^a}{2}\left( \frac{\partial \hat{u}_k}{\partial x_2} \right) \tag{15}$$
$$u_k^{(3)}\left( \frac{R_i^a \sqrt{3}}{2}, x_2 \right) = u_k^{(3)}\left( -\frac{R_i^a \sqrt{3}}{2}, x_2 \right) + R_i^a \sqrt{3}\left( \frac{\partial \hat{u}_k}{\partial x_1} \right)$$

Three different sets of displacement boundary conditions were applied to the RVE in this study. Each set is discussed below.

*4.4.1 Case I: uniaxial displacements along $(n_1,0)$*

A macroscopic graphene sheet is subjected to uniaxial loading conditions as shown in Figure 6. An axial displacement $\Delta$ is prescribed on the upper edge while the lower edge is constrained. The displacement is relatively small and the $h \times w$ plate is perfectly elastic. If it is assumed that the global displacements $\hat{u}_1$ and $\hat{u}_2$ vary linearly over the global coordinates $\hat{x}_1$ and $\hat{x}_2$, then these displacements may be written as:

$$\hat{u}_1(\hat{x}_k) = B_1 \hat{x}_1 + B_2$$
$$\hat{u}_2(\hat{x}_k) = B_3 \hat{x}_2 + B_4 \tag{16}$$

where $B_1$, $B_2$, $B_3$, and $B_4$ are constants which depend on the geometry and applied global displacements. The boundary conditions for this case are:

$$\hat{u}_2\left(\hat{x}_1, \frac{h}{2}\right) = \Delta$$
$$\hat{u}_2\left(\hat{x}_1, -\frac{h}{2}\right) = 0 \tag{17}$$
$$\hat{u}_1\left(0, \hat{x}_2\right) = 0$$

Since small elastic displacements are assumed, the strains and constitutive equations are [38]:

$$\varepsilon_1 = \frac{\partial \hat{u}_1}{\partial \hat{x}_1} \quad \varepsilon_2 = \frac{\partial \hat{u}_2}{\partial \hat{x}_2}$$
$$\varepsilon_{11} = \frac{1}{Y^g}\left(\sigma_{11} - \nu^g \sigma_{22}\right) \quad \varepsilon_{22} = \frac{1}{Y^g}\left(\sigma_{22} - \nu^g \sigma_{11}\right) \tag{18}$$

where $\varepsilon_{11}$ and $\varepsilon_{22}$ are normal strains, and $\sigma_{11}$, and $\sigma_{22}$ are normal stresses in the plate. Substitution of equations (17) and (18) into equation (16) and solving for the constants $B_1$, $B_2$, $B_3$, and $B_4$ results in the following displacement functions:

$$\hat{u}_1\left(\hat{x}_k\right) = -\frac{\nu^g \Delta}{h}\hat{x}_1$$
$$\hat{u}_2\left(\hat{x}_k\right) = \frac{\Delta}{h}\hat{x}_2 + \frac{\Delta}{2} \tag{19}$$

The global and RVE coordinates are related by:

$$\hat{x}_k = x_k + f_k \tag{20}$$

where $f_k$ is a vector indicating the relative position of the two coordinate systems with respect to each other. Using equations (15), (19), and (20), the RVE boundary displacements are determined to be:

$$
\begin{aligned}
u_1^{(1)}\left(-\sqrt{3}x_2-\frac{R_l^a\sqrt{3}}{2},x_2+\frac{3R_l^a}{2}\right)&=u_1^{(1)}\left(-\sqrt{3}x_2-\sqrt{3}R_l^a,x_2\right)-\frac{\nu^g R_l^a\sqrt{3}\Delta}{2h}\\
u_2^{(1)}\left(-\sqrt{3}x_2-\frac{R_l^a\sqrt{3}}{2},x_2+\frac{3R_l^a}{2}\right)&=u_2^{(1)}\left(-\sqrt{3}x_2-\sqrt{3}R_l^a,x_2\right)+\frac{3R_l^a\Delta}{2h}\\
u_1^{(2)}\left(\sqrt{3}x_2+\frac{R_l^a\sqrt{3}}{2},x_2+\frac{3R_l^a}{2}\right)&=u_1^{(2)}\left(\sqrt{3}x_2+\sqrt{3}R_l^a,x_2\right)+\frac{\nu^g R_l^a\sqrt{3}\Delta}{2h}\\
u_2^{(2)}\left(\sqrt{3}x_2+\frac{R_l^a\sqrt{3}}{2},x_2+\frac{3R_l^a}{2}\right)&=u_2^{(2)}\left(\sqrt{3}x_2+\sqrt{3}R_l^a,x_2\right)+\frac{3R_l^a\Delta}{2h}\\
u_1^{(3)}\left(\frac{R_l^a\sqrt{3}}{2},x_2\right)&=u_1^{(3)}\left(-\frac{R_l^a\sqrt{3}}{2},x_2\right)-\frac{\nu^g R_l^a\sqrt{3}\Delta}{h}\\
u_2^{(3)}\left(\frac{R_l^a\sqrt{3}}{2},x_2\right)&=u_2^{(3)}\left(-\frac{R_l^a\sqrt{3}}{2},x_2\right)
\end{aligned}
\tag{21}
$$

*4.4.2 Case II: uniaxial displacements along $(0,n_1)$*

The same macroscopic graphene sheet studied in Case I is now subjected to a different set of displacements, as shown in Figure 7. The boundary conditions for this case are:

$$
\begin{aligned}
\hat{u}_1\left(\frac{w}{2},\hat{x}_2\right)&=\Delta\\
\hat{u}_1\left(-\frac{w}{2},\hat{x}_2\right)&=0\\
\hat{u}_2\left(\hat{x}_1,0\right)&=0
\end{aligned}
\tag{22}
$$

If the same assumptions are made for this case as for Case I, then equations (16), (18), and (22) may be used to determine the following global displacements:

$$
\begin{aligned}
\hat{u}_1\left(\hat{x}_k\right)&=\frac{\Delta}{w}\hat{x}_1+\frac{\Delta}{2}\\
\hat{u}_2\left(\hat{x}_k\right)&=-\frac{\nu^g\Delta}{w}\hat{x}_2
\end{aligned}
\tag{23}
$$

Using equations (15), (20), and (23), the RVE boundary displacements are determined to be:

$$
\begin{aligned}
u_1^{(1)}\left(-\sqrt{3}x_2-\frac{R_i^a\sqrt{3}}{2},x_2+\frac{3R_i^a}{2}\right)&=u_1^{(1)}\left(-\sqrt{3}x_2-\sqrt{3}R_i^a,x_2\right)+\frac{R_i^a\sqrt{3}\Delta}{2w}\\
u_2^{(1)}\left(-\sqrt{3}x_2-\frac{R_i^a\sqrt{3}}{2},x_2+\frac{3R_i^a}{2}\right)&=u_2^{(1)}\left(-\sqrt{3}x_2-\sqrt{3}R_i^a,x_2\right)-\frac{\nu^g 3R_i^a\Delta}{2w}\\
u_1^{(2)}\left(\sqrt{3}x_2+\frac{R_i^a\sqrt{3}}{2},x_2+\frac{3R_i^a}{2}\right)&=u_1^{(2)}\left(\sqrt{3}x_2+\sqrt{3}R_i^a,x_2\right)-\frac{R_i^a\sqrt{3}\Delta}{2w}\\
u_2^{(2)}\left(\sqrt{3}x_2+\frac{R_i^a\sqrt{3}}{2},x_2+\frac{3R_i^a}{2}\right)&=u_2^{(2)}\left(\sqrt{3}x_2+\sqrt{3}R_i^a,x_2\right)-\frac{\nu^g 3R_i^a\Delta}{2w}\\
u_1^{(3)}\left(\frac{R_i^a\sqrt{3}}{2},x_2\right)&=u_1^{(3)}\left(-\frac{R_i^a\sqrt{3}}{2},x_2\right)+\frac{R_i^a\sqrt{3}\Delta}{w}\\
u_2^{(3)}\left(\frac{R_i^a\sqrt{3}}{2},x_2\right)&=u_2^{(3)}\left(-\frac{R_i^a\sqrt{3}}{2},x_2\right)
\end{aligned}
\tag{24}
$$

*4.4.3 Case III: (pure-shear displacements)*

The macroscopic graphene sheet is now subjected to pure shear, as indicated in Figure 8. The constraints imposed for in-plane shear loading assume that the shearing faces normal to the direction of the applied shear are displaced by identical amounts. The displacement is relatively small and the $h\times w$ plate is perfectly elastic. If it is assumed that the global displacements $\hat{u}_1$ and $\hat{u}_2$ vary linearly over $\hat{x}_1$ and $\hat{x}_2$, then these displacements may be written as:

$$
\begin{aligned}
\hat{u}_1(\hat{x}_k)&=B_5\hat{x}_1+B_6\hat{x}_2+B_7\\
\hat{u}_2(\hat{x}_k)&=B_8\hat{x}_1+B_9\hat{x}_2+B_{10}
\end{aligned}
\tag{25}
$$

The boundary conditions are:

$$
\begin{aligned}
&\hat{u}_1\left(-\frac{w}{2},\hat{x}_2\right)=0 \quad \hat{u}_1\left(\frac{w}{2},\hat{x}_2\right)=0\\
&\hat{u}_2\left(-\frac{w}{2},\hat{x}_2\right)=0 \quad \hat{u}_2\left(\frac{w}{2},\hat{x}_2\right)=\Delta\\
&\hat{u}_1\left(\hat{x}_1,\frac{h}{2}\right)=\hat{u}_1\left(\hat{x}_1,-\frac{h}{2}\right)\\
&\hat{u}_2\left(\hat{x}_1,\frac{h}{2}\right)=\hat{u}_2\left(\hat{x}_1,-\frac{h}{2}\right)
\end{aligned}
\tag{26}
$$

Substitution of equation (26) into equation (25) results in:

$$\hat{u}_1(\hat{x}_k) = 0$$
$$\hat{u}_2(\hat{x}_k) = \frac{\Delta}{w}\hat{x}_1 + \frac{\Delta}{2} \tag{27}$$

Using equations (15), (20), and (27), the RVE boundary displacements may be determined:

$$u_1^{(1)}\left(-\sqrt{3}x_2 - \frac{R_i^a\sqrt{3}}{2}, x_2 + \frac{3R_i^a}{2}\right) = u_1^{(1)}\left(-\sqrt{3}x_2 - \sqrt{3}R_i^a, x_2\right)$$
$$u_2^{(1)}\left(-\sqrt{3}x_2 - \frac{R_i^a\sqrt{3}}{2}, x_2 + \frac{3R_i^a}{2}\right) = u_2^{(1)}\left(-\sqrt{3}x_2 - \sqrt{3}R_i^a, x_2\right) + \frac{R_i^a\sqrt{3}\Delta}{2w}$$
$$u_1^{(2)}\left(\sqrt{3}x_2 + \frac{R_i^a\sqrt{3}}{2}, x_2 + \frac{3R_i^a}{2}\right) = u_1^{(2)}\left(\sqrt{3}x_2 + \sqrt{3}R_i^a, x_2\right)$$
$$u_2^{(2)}\left(\sqrt{3}x_2 + \frac{R_i^a\sqrt{3}}{2}, x_2 + \frac{3R_i^a}{2}\right) = u_2^{(2)}\left(\sqrt{3}x_2 + \sqrt{3}R_i^a, x_2\right) - \frac{R_i^a\sqrt{3}\Delta}{2w} \tag{28}$$
$$u_1^{(3)}\left(\frac{R_i^a\sqrt{3}}{2}, x_2\right) = u_1^{(3)}\left(-\frac{R_i^a\sqrt{3}}{2}, x_2\right)$$
$$u_2^{(3)}\left(\frac{R_i^a\sqrt{3}}{2}, x_2\right) = u_2^{(3)}\left(-\frac{R_i^a\sqrt{3}}{2}, x_2\right) + \frac{R_i^a\sqrt{3}\Delta}{w}$$

To simplify the application of equations (21), (24), and (28) to finite element boundary conditions, without loss of generality, the following assumption can be made:

$$\hat{u}_k\left(x_m + d_m^{(\alpha)}\right) = -\hat{u}_k(x_m) \tag{29}$$

### 4.5 Finite element modeling

The truss and continuum representations of the RVE were modeled using ANSYS® 5.4 [39]. In the truss model, each pin-jointed extensible rod was modeled using a finite truss element (LINK1) with two degrees of freedom at each node (displacements parallel to $x_1$ and $x_2$). Rod types *a* and *b* were assumed to have the same cross-sectional area and different Young's moduli. The entire RVE was modeled with the cross-sectional areas of the type *a* rods divided by a factor of 2, since these rods are sharing their total area with adjacent RVEs. The equivalent-plate RVE was modeled by using two plane-stress 4-noded quadrilateral elements (PLANE42) with linear displacement fields on the edges (Figure 3). The boundary conditions described above were applied to each node for a macroscopic graphene sheet height, width, and displacement of $1\text{x}10^6$ nm, $1\text{x}10^6$ nm, and 100 nm (corresponding to global uniaxial and shear strains of 0.01%), respectively. For both models, the total strain energy of each element was calculated for the given boundary conditions, then summed to obtain the strain energy of the entire RVE model. A systematic variation of thickness was used to calculate the strain energy of the equivalent plate,

and an iterative process was used to find the critical thickness (accurate to 0.01 nm) that resulted in the equivalence of the strain energies of the truss and equivalent-plate models.

## 5. Discussion

Using the method described herein, effective thicknesses were determined for the three loading cases. For loading cases I and II, the resulting effective thickness was calculated to be 0.28 nm. For load case III, the effective thickness was 0.24 nm. These values are close to, but smaller than, the widely accepted value of the graphitic interatomic spacing, 0.34 nm, and much larger than the value suggested by Yakobson *et al.* [15], 0.066 nm. Even though there is a difference in the effective plate thickness based on different loading conditions, the difference is very small compared to the range of values currently used.

It may be assumed that the Young's modulus of a carbon nanotube can be calculated using:

$$Y''' \propto (A''')^{-1} \tag{30}$$

where $A'''$ is the cross-sectional area of the hollow continuum cylinder with a constant mid-plane radius, $r'$. The inner radius, $r''$, and outer radius, $r'''$, of the tube are:

$$\begin{aligned} r'' &= r' - \frac{t}{2} \\ r''' &= r' + \frac{t}{2} \end{aligned} \tag{31}$$

where $t$ is the wall thickness. The cross-sectional area of the hollow continuum cylinder is:

$$A''' = 2\pi t r' \tag{32}$$

The calculated cross-sectional areas are shown in Table 1. The percentage difference in the calculated Young's modulus based on the effective thickness obtained for the three load cases with respect to the interatomic spacing is also shown in Table 1. The results suggest that measured and calculated values of physical and mechanical properties of carbon nanotubes that are dependent on the dimensions of the continuum tube may differ significantly based on the assumed geometry.

The proposed method for continuum modeling may be applied to other nano-structured materials such as nanotube-reinforced polymer composites and will yield satisfactory results if the right assumptions are made. If the material is subjected to large deformations such that non-linear deformation and failure are key issues, then the particular approximations made in this study may not be appropriate.

## 6. Conclusions

A method has been presented for modeling structure-property relationships of nano-structured materials. This method serves to link computational chemistry, which is used to predict molecular properties, and solid mechanics, which describes macroscopic mechanical behavior based on macroscopic material properties. This link is established by replacing discrete molecular structures with equivalent-continuum models. It has been shown that this replacement may be accomplished by equating the vibrational potential energy of nano-structured materials with the mechanical strain energy of representative truss and continuum models.

As an important example with direct applications to the development and characterization of carbon nanotubes, the model has been applied to determine the effective geometry of a graphene sheet. A representative volume element (RVE) of the chemical structure of graphene has been substituted with RVEs of equivalent-truss and equivalent-continuum models. As a result, an effective thickness of the continuum model has been determined. This effective thickness has been shown to be similar to, but slightly smaller than, the interatomic spacing of graphite.

## Acknowledgements

This work was performed while Dr. Odegard and Dr. Wise held National Research Council Research Associateship Awards at NASA Langley Research Center.

## References

[1] Edelstein, A.S. and Cammarata, R.C.: *Nanomaterials: Synthesis, Properties and Applications*. Bristol: Institute of Physics Publishing, 1996.

[2] Treacy, M.M.J.; Ebbesen, T.W., and Gibson, J.M.: Exceptionally high Young's Modulus Observed for Individual Carbon Nanotubes. *Nature*. Vol. 381, 1996, pp. 678-680.

[3] Krishnan, A.; Dujardin, E.; Ebbesen, T.W.; Yianilos, P.N., and Treacy, M.M.J.: Young's Modulus of Single-Walled Nanotubes. *Physical Review B*. Vol. 58, no. 20, 1998, pp. 14013-14019.

[4] Salvetat, J.P.; Bonard, J.M.; Thomson, N.H.; Kulik, A.J.; Forro, L.; Benoit, W., and Zuppiroli, L.: Mechanical Properties of Carbon Nanotubes. *Applied Physics A*. Vol. 69. 1999, pp. 255-260.

[5] Yu, M.; Dyer, M.J.; Skidmore, G.D.; Rohrs, H.W.; Lu, X.; Ausman, K.D.; Von Ehr, J.R., and Ruoff, R.S.: Three-Dimensional Manipulation of carbon nanotubes under a scanning electron microscope. *Nanotechnology*. Vol. 10, 1999, pp. 244-252.

[6] Yu, M.; Lourie, O.; Dyer, M.J.; Moloni, K.; Kelly, T.F., and Ruoff, R.S.: Strength and Breaking Mechanism of Multiwalled Carbon Nanotubes Under Tensile Load. *Science*. Vol. 287, 2000, pp. 637-640.

[7] Lu, J.P.: Elastic Properties of Carbon Nanotubes and Nanoropes. *Physical Review Letters*. Vol. 79, no. 7, 1997, pp. 1297-1300.

[8] Hernandez, E.; Goze, C.; Bernier, P., and Rubio, A.: Elastic Properties of C and $B_xC_yN_z$ Composite Nanotubes. *Physical Review Letters*. Vol. 80, no. 20, 1998, pp. 4502-4505.

[9] Yao, N. and Lordi, V.: Young's Modulus of Single-Walled Carbon Nanotubes. *Journal of Applied Physics*. Vol. 84, no. 4, 1998, pp. 1939-1943.

[10] Ozaki, T.; Iwasa, Y., and Mitani, T.: Stiffness of Single-Walled Carbon Nanotubes under Large Strain. *Physical Review Letters*. Vol. 84, no. 8, 2000, pp. 1712-1715.

[11] Van Lier, G.; Van Alsenoy, C.; Van Doren, V., and Geerlings, P.: Ab initio Study of the Elastic Properties of Single-Walled Carbon Nanotubes and Graphene. *Chemical Physics Letters*. Vol. 326, 2000, pp. 181-185.

[12] Cornwell, C.F. and Wille, L.T.: Elastic Properties of Single-Walled Carbon Nanotubes in Compression. *Solid State Communications*. Vol. 101, no. 8, 1997, pp. 555-558.

[13] Wong, E.W.; Sheehan, P.E., and Leiber, C.M.: Nanobeam Mechanics: Elasticity, Strength, and Toughness of Nanorods and Nanotubes. *Science*. Vol. 277, 1997, pp. 1971-1975.

[14] Govindjee, S. and Sackman, J.L.: On the Use of Continuum Mechanics to Estimate the Properties of Nanotubes. *Solid State Communications*. Vol. 110, 1999, pp. 227-230.

[15] Yakobson, B.I.; Brabec, C.J., and Bernholc, J.: Nanomechanics of Carbon Tubes: Instabilities beyond Linear Response. *Physical Review Letters*. Vol. 76, no. 14, 1996, pp. 2511-2514.

[16] Ru, C.Q.: Effect of Van der Waals Forces on Axial Buckling of a Double-Walled Carbon Nanotube. *Journal of Applied Physics*. Vol. 87, no. 10, 2000, pp. 7227-7231.

[17] Ru, C.Q.: Effective Bending Stiffness of Carbon Nanotubes. *Physical Review B*. Vol. 62, no. 15, 2000, pp. 9973-9976.

[18] Robertson, D.H.; Brenner, D.W., and Mintmire, J.W.: Energetics of nanoscale graphitic tubules. *Physical Review B*. Vol. 45, no. 21, 1992, pp. 12592-12595.

[19] Halicioglu, T.: Stress Calculations for Carbon Nanotubes. *Thin Solid Films*. Vol. 312, 1998, pp. 11-14.

[20] Rappe, A.K. and Casewit, C.J.: *Molecular Mechanics Across Chemistry*. Sausalito, California: University Science Books, 1997.

[21] Born, M. and Huang, K.: *Dynamical Theory of Crystal Lattices*. London: Oxford University Press, 1954.

[22] Noor, A.K.; Anderson, M.S., and Greene, W.H.: Continuum Models for Beam- and Platelike Lattice Structures. *AIAA Journal*. Vol. 16, no. 12, 1978, pp. 1219-1228.

[23] Sun, C.T.; Kim, B.J., and Bogdanoff, J.L.: On the Derivation of Equivalent Simple Models for Beam and Plate-Like Structures in Dynamic Analysis. *AIAA/ASME/ASCE/AHS 22nd Structures, Structural Dynamics & Materials Conference*. Atlanta, Georgia: 1981.

[24] Noor, A.K.: Continuum Modeling for Repetitive Lattice Structures. *ASME Applied Mechanics Reveiws*. Vol. 41, no. 7, 1988, pp. 285-296.

[25] Dow, J.O. and Huyer, S.A.: Continuum Models of Space Station Structures. *Journal of Aerospace Engineering*. Vol. 2, no. 4, 1989, pp. 220-238.

[26] Sun, C.T. and Leibbe, S.W.: Global-Local Approach to Solving Vibration of Large Truss Structures. *AIAA Journal*. Vol. 28, no. 2, 1990, pp. 303-308.

[27] Lee, U.: Equivalent Continuum Models of Large Plate-like Lattice Structures. *International Journal of Solids and Structures*. Vol. 31, no. 4, 1994, pp. 457-467.

[28] Eringen, A.C.: Linear Theory of Micropolar Elasticity. *Journal of Mathematics and Mechanics*. Vol. 15, no. 6, 1966, pp. 909-923.

[29] Allinger, N.L.; Yuh, Y.H., and Lii, J.H.: Molecular Mechanics. The MM3 Force Field for Hydrocarbons. *Journal of the American Chemical Society*. Vol. 111, 1989, pp. 8551-8566.

[30] Lii, J.H. and Allinger, N.L.: Molecular Mechanics. The MM3 Force Field for Hydrocarbons. 2. Vibrational Frequencies and Thermodynamics. *Journal of the American Chemical Society*. Vol. 111, 1989, pp. 8566-8575.

[31] Lii, J.H. and Allinger, N.L.: Molecular Mechanics. The MM3 Force Field for Hydrocarbons. 3. The van der Waals' Potentials and Crystal Data for Aliphatic and Aromatic Hydrocarbons. *Journal of the American Chemical Society*. Vol. 111, 1989, pp. 8576-8582.

[32] Zienkiewicz, O.C.: *The Finite Element Method in Engineering Science*. London: McGraw-Hill Publishing Company Limited, 1971.

[33] Kelly, B.T.: *Physics of Graphite*. Essex, England: Applied Science Publishers LTD, 1981.

[34] Pierson, H.O.: *Handbook of Carbon, Graphite, Diamond and Fullerenes: Properties, Processing and Applications*. New Jersey: Noyes Publications, 1993.

[35] Harris, P.J.F.: *Carbon Nanotubes and Related Structures: New Materials for the Twenty-first Century*. Cambridge: Cambridge University Press, 1999.

[36] Whitcomb, J.D.; Chapman, C.D., and Tang, X.: Derivation of Boundary Conditions for Micromechanics Analyses of Plain and Satin Weave Composites. *Journal of Composite Materials*. Vol. 34, no. 9, 2000, pp. 724-747.

[37] Chapman, C.D. and Whitcomb, J.D.: Thermally Induced Damage Initiation and Growth in Plain and Satin Weave Carbon-Carbon Composites. *Mechanics of Composite Materials and Structures*. Vol. 7, no. 2, 2000, pp. 177-194.

[38] Timoshenko, S. and Goodier, J.N.: *Theory of Elasticity*. New York: McGraw-Hill Book Company, 1951.

[39] SAS IP, Inc.: Canonsburg, PA, 1997.

| | continuum wall thickness [nm] | continuum cross-sectional area [$nm^2$] | % difference of Young's modulus [%] |
|---|---|---|---|
| load cases I and II | 0.28 | 1.76r' | 21 |
| load case III | 0.24 | 1.51r' | 42 |
| average of I, II, and III | 0.27 | 1.70r' | 26 |
| interatomic spacing | 0.34 | 2.14r' | - |

Table 1 – Percent difference in calculated Young's modulus for different wall thicknesses with respect to the Young's modulus calculated with the interatomic spacing.

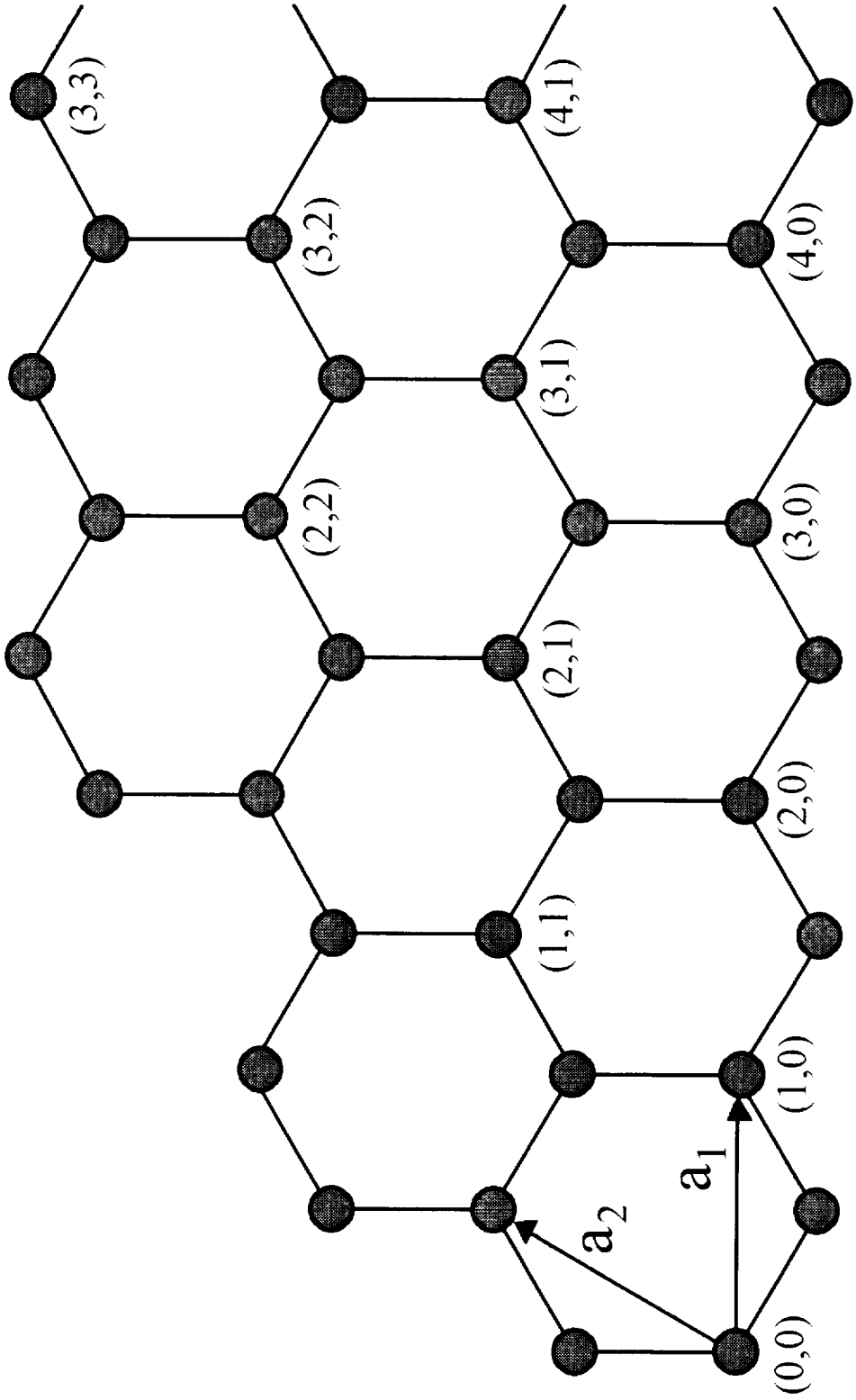


Figure 1 – Unit vector notation for a graphene sheet

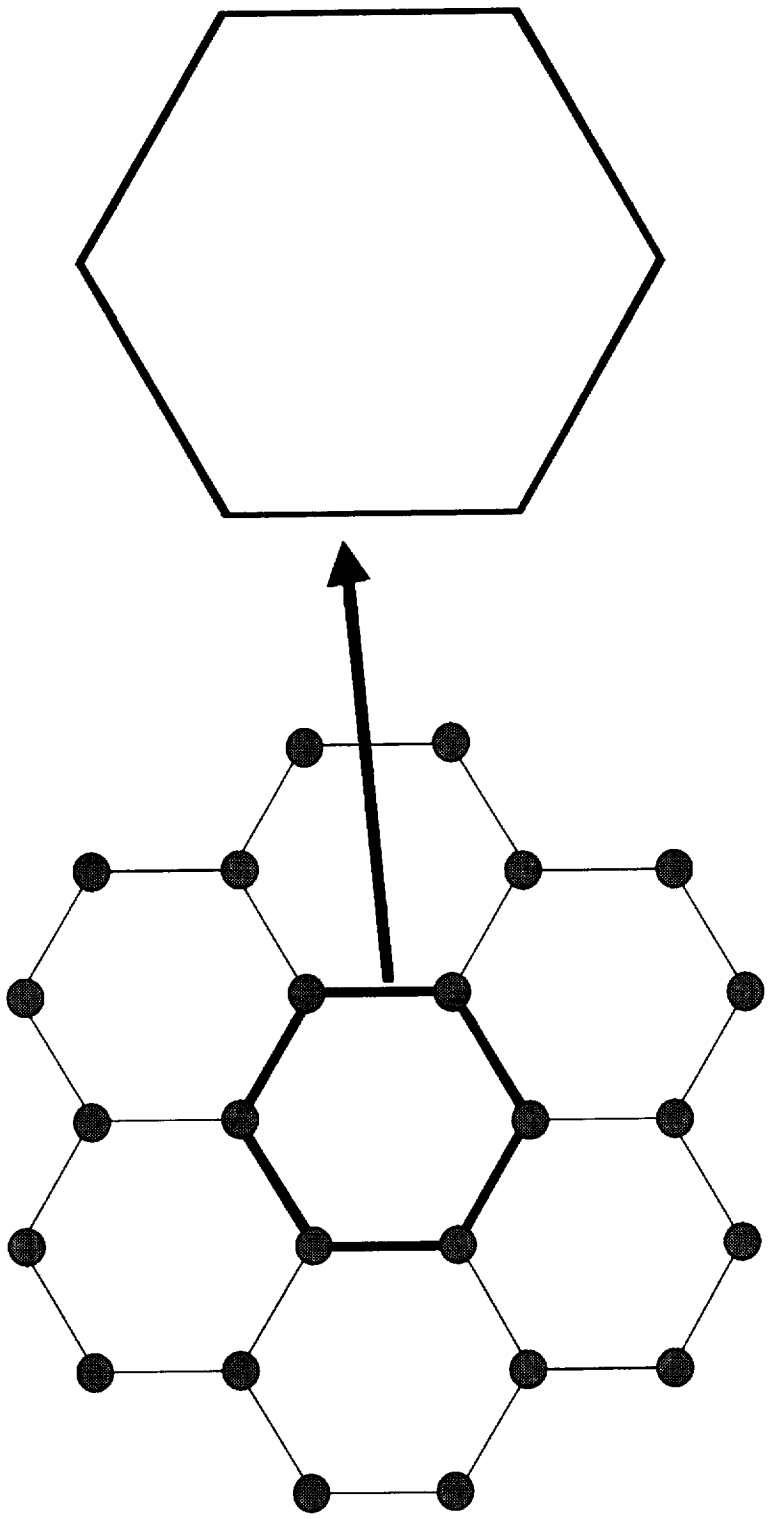

Figure 2 – Representative volume element of a graphene sheet

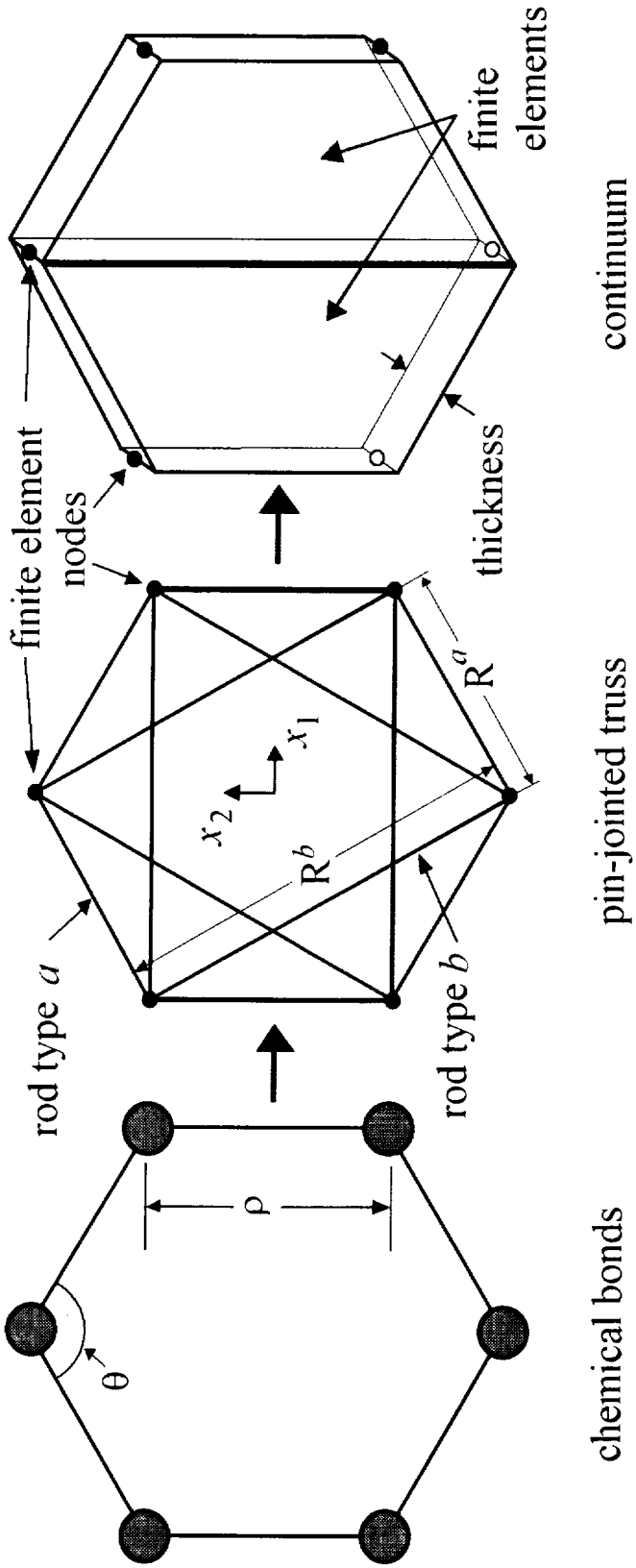


Figure 3 – Representative volume elements for the chemical, truss, and continuum models

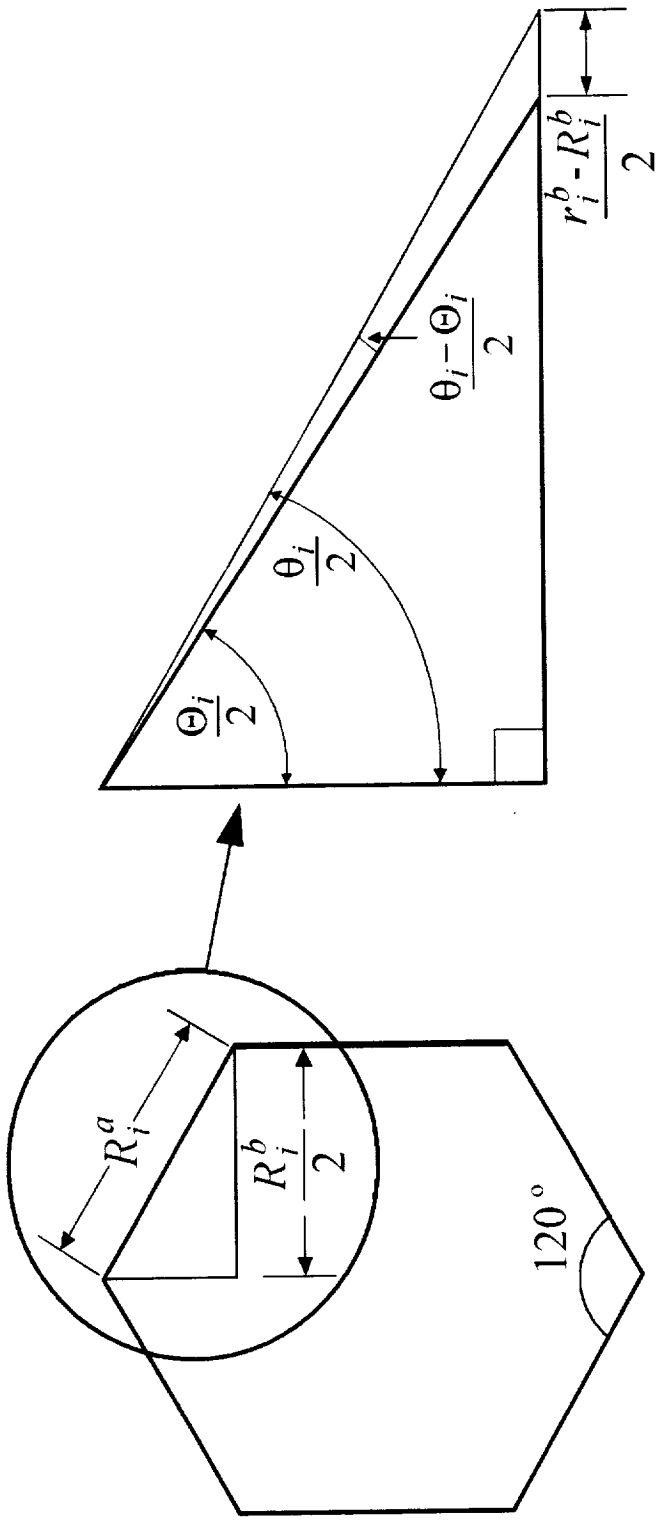


Figure 4 – Schematic of the geometry of deformation of the representative volume element

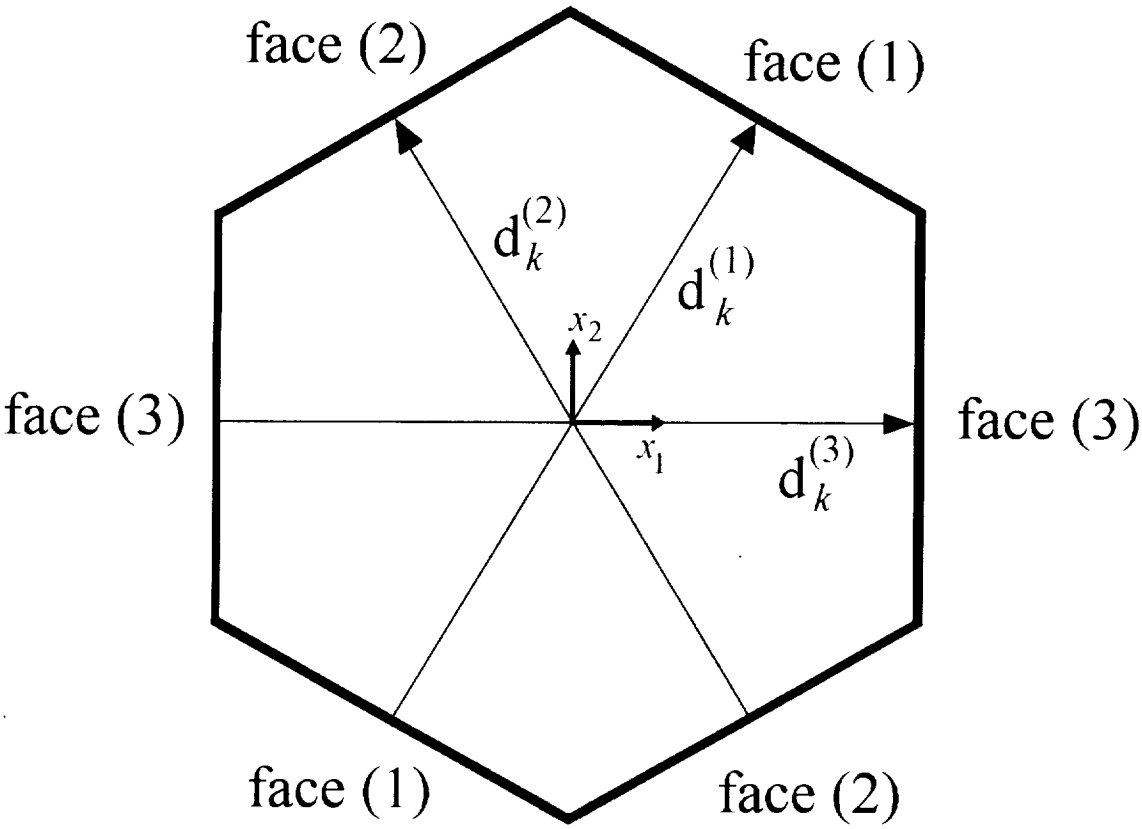


Figure 5 – Vectors of periodicity of the RVE

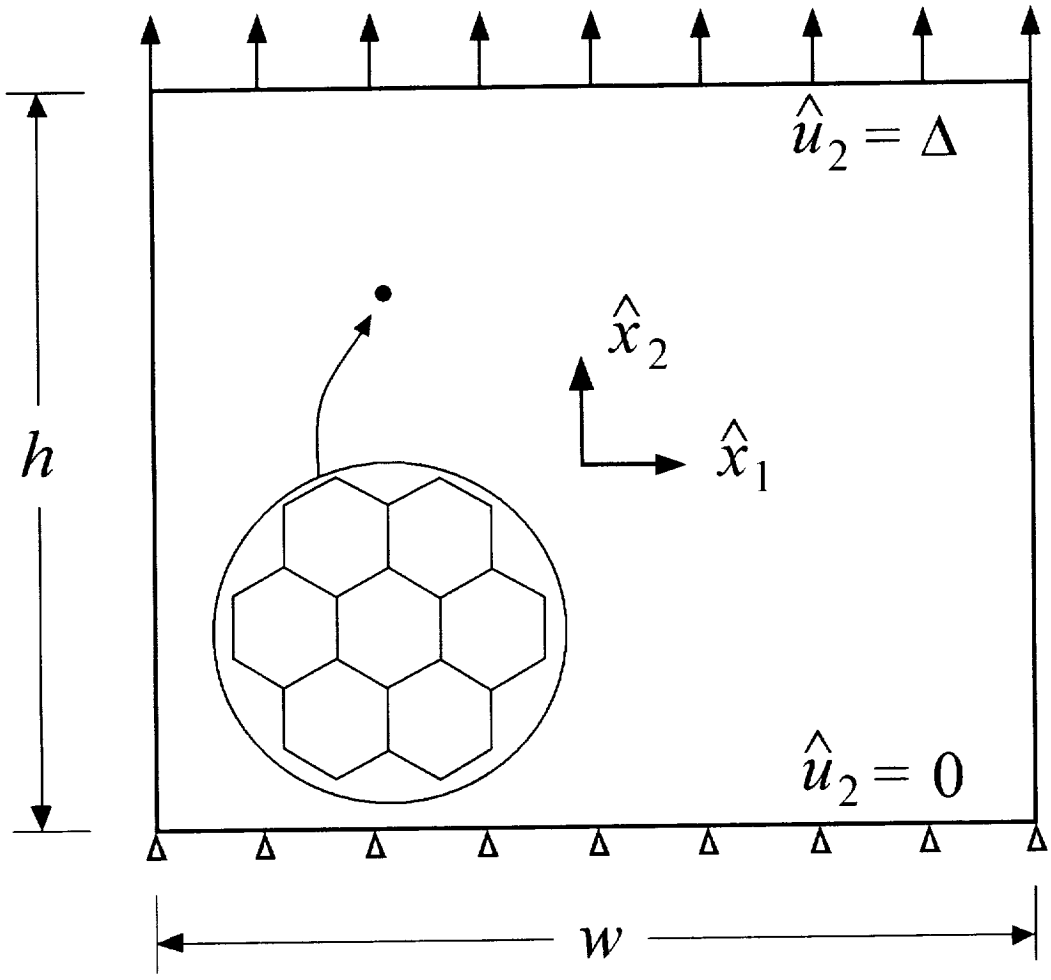


Figure 6 – Loading case I: uniaxial displacements along ($n_1$,0)

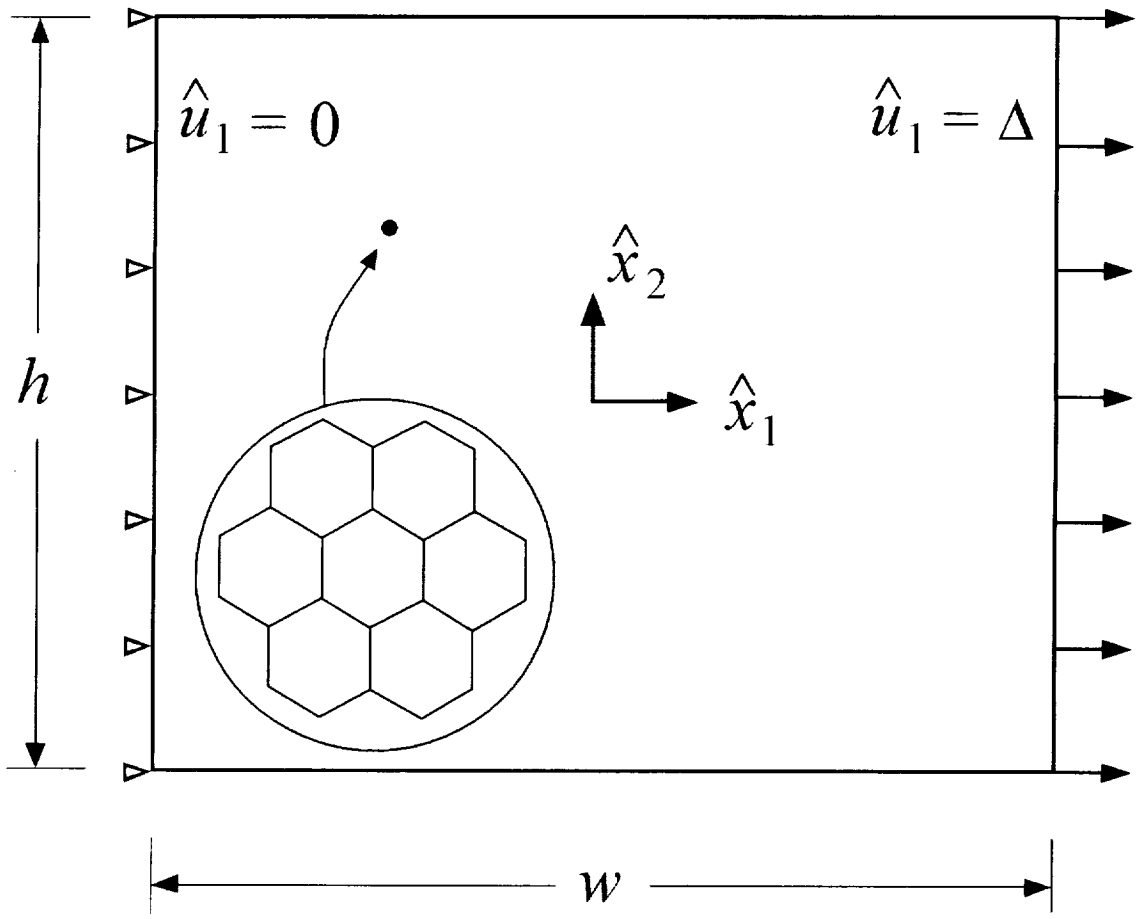


Figure 7 – Loading case II: uniaxial displacements along $(0,n_2)$

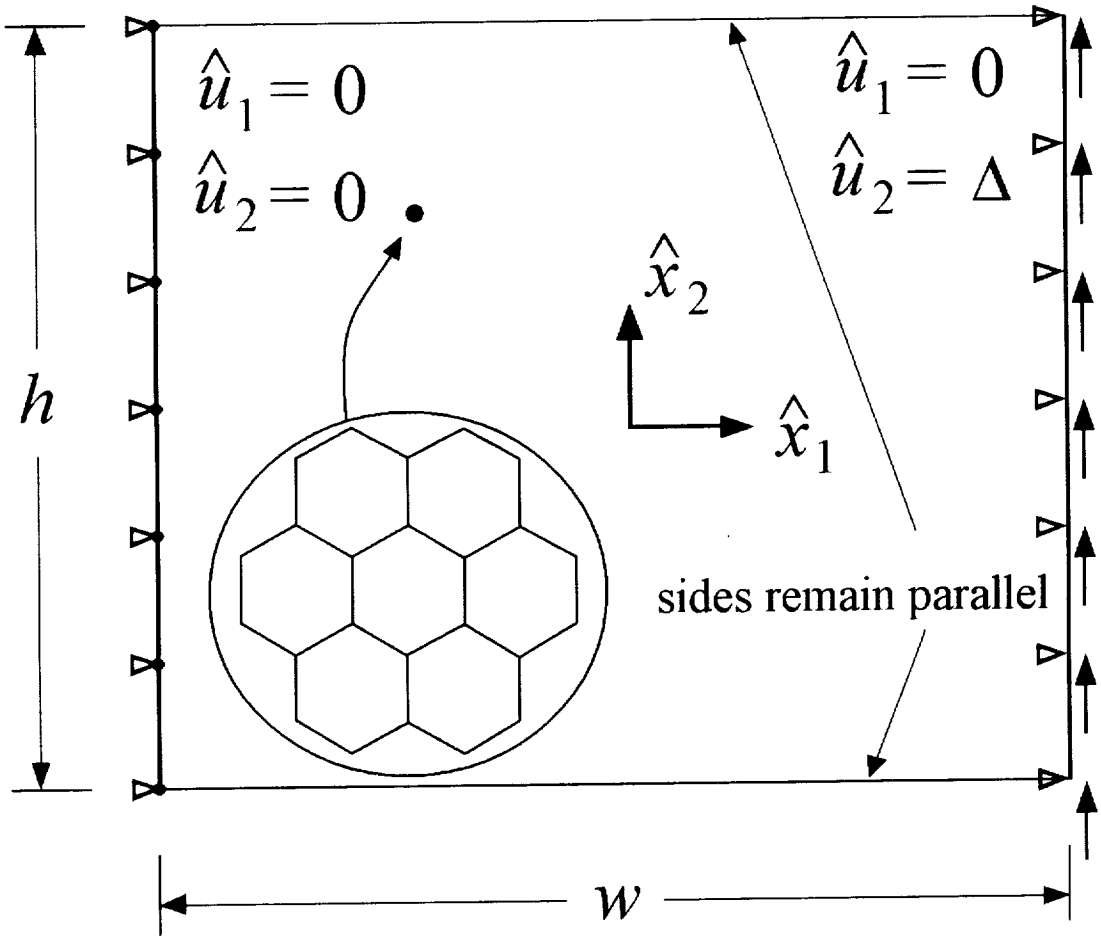


Figure 8 – Loading case III: pure shear displacements

# REPORT DOCUMENTATION PAGE

*Form Approved*
*OMB No. 0704-0188*



| 1. AGENCY USE ONLY (*Leave blank*) | 2. REPORT DATE | 3. REPORT TYPE AND DATES COVERED |
|---|---|---|
| | May 2001 | Technical Memorandum |

**4. TITLE AND SUBTITLE**
Equivalent-Continuum Modeling of Nano-Structured Materials

**5. FUNDING NUMBERS**
706-63-51-03

**6. AUTHOR(S)**
Gregory M. Odegard, Thomas S. Gates, Lee M. Nicholson and Kristopher E. Wise

**7. PERFORMING ORGANIZATION NAME(S) AND ADDRESS(ES)**
NASA Langley Research Center
Hampton, VA 23681-2199

**8. PERFORMING ORGANIZATION REPORT NUMBER**
L-18081

**9. SPONSORING/MONITORING AGENCY NAME(S) AND ADDRESS(ES)**
National Aeronautics and Space Administration
Washington, DC 20546-0001

**10. SPONSORING/MONITORING AGENCY REPORT NUMBER**
NASA/TM-2001-210863

**11. SUPPLEMENTARY NOTES**
This work was performed while Dr. Odegard and Dr. Wise held National Research Council Research Associateship Awards at NASA Langley Research Center

**12a. DISTRIBUTION/AVAILABILITY STATEMENT**
Unclassified-Unlimited
Subject Category 27 Distribution: Standard
Availability: NASA CASI (301) 621-0390

**12b. DISTRIBUTION CODE**

**13. ABSTRACT** (*Maximum 200 words*)
A method has been developed for modeling structure-property relationships of nano-structured materials. This method serves as a link between computational chemistry and solid mechanics by substituting discrete molecular structures with an equivalent-continuum model. It has been shown that this substitution may be accomplished by equating the vibrational potential energy of a nano-structured material with the strain energy of representative truss and continuum models. As an important example with direct application to the development and characterization of single-walled carbon nanotubes, the model has been applied to determine the effective continuum geometry of a graphene sheet. A representative volume element of the equivalent-continuum model has been developed with an effective thickness. This effective thickness has been shown to be similar to, but slightly smaller than, the interatomic spacing of graphite.

**14. SUBJECT TERMS**
nanotechnology, nanotubes, continuum mechanics, molecular mechanics, finite elements

**15. NUMBER OF PAGES**
35

**16. PRICE CODE**
A03

| 17. SECURITY CLASSIFICATION OF REPORT | 18. SECURITY CLASSIFICATION OF THIS PAGE | 19. SECURITY CLASSIFICATION OF ABSTRACT | 20. LIMITATION OF ABSTRACT |
|---|---|---|---|
| Unclassified | Unclassified | Unclassified | UL |